Clinical Neurophysiology 142 (2022) 11–19

Contents lists available at ScienceDirect

Clinical Neurophysiology

journal homepage: www.elsevier.com/locate/clinph

Microscale electrophysiological functional connectivity in human cortico-basal ganglia network

Ashley C Guest [a,b,1], Kevin J O'Neill III [b,1], Dakota Graham [b], Zaman Mirzadeh [c], Francisco A Ponce [c], Bradley Greger [b,*]

[a] College of Medicine—Phoenix, University of Arizona, Phoenix, AZ 85004, USA
[b] School of Biological Health Systems Engineering, Arizona State University, Tempe, AZ 85281, USA
[c] Barrow Center for Neuromodulation, Barrow Neurological Institute, St. Joseph's Hospital and Medical Center, Phoenix, AZ 85013, USA

ARTICLE INFO

Article history:
Accepted 30 June 2022
Available online 16 July 2022

Keywords:
Parkinson's disease
Microcircuit
Subthalamic nucleus
Cortex
Deep brain stimulation
Local field potential

HIGHLIGHTS

- Action potentials (AP) from subthalamic nucleus (STN) neurons were significantly related to local field potentials in STN and motor cortex.
- Functional connectivity between STN neuron APs and cortical local field potentials was topographically organized on a sub-centimeter scale.
- This spatial specificity of functional connectivity was different for different subthalamic neurons, including neighboring subthalamic neurons.

ABSTRACT

Objective: We investigated the electrophysiological relationships in the cortico-basal ganglia network on a sub-centimeter scale to increase our understanding of neural functional relationships in Parkinson's disease (PD).
Methods: Data was intraoperatively recorded from 2 sources in the human brain—a microelectrode in the subthalamic nucleus (STN) and a micro-electrocorticography grid on the motor association cortex—during bilateral deep brain stimulation (DBS) electrode placement. STN neurons and local field potential (LFP) were defined as functionally connected when the 99.7% confidence intervals of the action potential (AP)-aligned average LFP and control did not overlap.
Results: APs from STN neurons were functionally connected to the STN LFP for 18/46 STN neurons. This functional connection was observed between STN neuron APs and cortical LFP for 25/46 STN neurons. The cortical patterns of electrophysiological functional connectivity differed for each neuron.
Conclusions: A subset of single neurons in the STN exhibited functional connectivity with electrophysiological activity in the STN and at a distance with the motor association cortex surveyed on a sub-centimeter spatial scale. These connections show a per neuron differential topography on the cortex.
Significance: The cortico-basal ganglia circuit is organized on a sub-centimeter scale, and plays an important role in the mechanisms of PD and DBS.

1. Introduction

The anatomical and physiological relationships in the cortico-basal ganglia circuit are critical components of motor information processing and play an integral role in the mechanism of deep brain stimulation (DBS) for Parkinson's disease (PD; Eisinger et al., 2019; Okun, 2012). The anatomy of the cortico-basal ganglia circuit portrays intricate relationships between several structures

Abbreviations: DBS, deep brain stimulation; PD, Parkinson's disease; STN, subthalamic nucleus; AP, action potential; LFP, local field potential; ECoG, electrocorticography; GPi, globus pallidus internus; ISI, inter-spike interval; MRI, magnetic resonance imaging; CT, computerized tomography; IRB, institutional review board.

* Corresponding author.
E-mail address: bradley.greger@asu.edu (B. Greger).

[1] These authors contributed equally to this work.

https://doi.org/10.1016/j.clinph.2022.06.017
1388-2457/

interacting with each other to control movement (Albin et al., 1995; Eisinger et al., 2019; Obeso et al., 2000). Some of these structures, such as the subthalamic nucleus (STN) and globus pallidus internus (GPi) have become important targets for DBS treatment of movement disorders (Deuschl et al., 2006; Group, 2001; Herrington et al., 2016; Okun, 2012; Weaver et al., 2009). However, the functional relationship between these structures and the cortex is not completely understood, especially with regard to DBS treatment of PD. In particular, the cortex is often examined on a spatial scale much larger than the scale of cortical neural circuits. In this study, we examine the electrophysiological relationships in the cortico-basal ganglia network on a sub centimeter scale on the cortex in the context of patients with Parkinson's disease (PD) undergoing surgery for DBS electrode placement.

Though the mechanism of DBS is not entirely understood, the breadth of empirical evidence of the therapy's success using the STN or GPi (Deuschl et al., 2006; Group, 2001; Weaver et al., 2009) as targets and the evidence of cortical involvement (de Hemptinne et al., 2015; Miocinovic et al., 2018; Swann et al., 2018; Wang et al., 2018) speak to the importance of the cortico-basal ganglia circuit. Furthermore, activity in the premotor cortex is correlated with clinical outcomes, either with evoked potentials as intraoperative markers predicting efficacy (Miocinovic et al., 2018) or gamma activity as a feedback signal for adaptive DBS (Swann et al., 2018). One prominent theory regarding DBS is that it disrupts the hypersynchonous beta (12–35 Hz) field activity in the cortico-basal ganglia circuit (Heinrichs-Graham et al., 2014; Kühn et al., 2005; Whitmer et al., 2012), or locking between beta and higher frequencies (Cagnan et al., 2015; Cole et al., 2017; Lopez-Azcarate et al., 2010; Yang et al., 2014) There is enthusiasm for using beta activity in the STN as a feedback signal for adaptive DBS (Tinkhauser et al., 2017). However, recent work has shown that beta activity alone cannot explain all of the symptoms of PD (Devergnas et al., 2014; Quiroga-Varela et al., 2013; Swan et al., 2019; Zhang et al., 2018), with one group showing a link between theta (4–8 Hz) rhythms and tremor (Asch et al., 2020). We point to two areas that warrant further study of STN rhythms: examining the cortico-basal ganglia circuit on a fine spatial scale because of the non-uniformity of beta in the STN (Zhang et al., 2018), and studying a rhythms in the basal ganglia with a broadband perspective because of PD symptoms that cannot be sufficiently explained by beta (e.g. tremor) or are not treated DBS (e.g. gait problems, cognitive decline).

Cortical circuits on a micro- to mesoscale have been shown as essential components of neural networks in motor functioning, visual processing, and other sensory systems, and in the pathophysiology of neurodegenerative diseases (Krimer and Goldman-Rakic, 2001; McColgan et al., 2020; Mountcastle, 1997, 1956; Narayanan et al., 2015; Peters and Sethares, 1996). These micro- and meso-circuits are also major players in dysregulated neural systems in movement disorders (Amadeus Steiner et al., 2019; Farokhniaee and Lowery, 2021; Shimamoto et al., 2013). Examining cortical activity on a sub centimeter scale holds value in the effort to understand how cortical activity affects motor information processing, and how we can modulate it with DBS or other neuromodulatory therapies.

In the present study, we examine cortical circuits using micro-electrocorticography (micro-ECoG) grids (Shokoueinejad et al., 2019). Traditional ECoG electrodes integrate electrophysiological signals in a spatial region of 1–2 cm (Buzsáki et al., 2012; Kellis et al., 2016). A number of studies have demonstrated the spatial reach of local field potentials (LFP) is on a much smaller scale, somewhere between a few hundred microns to a few millimeters, inversely correlated with LFP frequency (Berens et al., 2008; Engel et al., 1990; Jia et al., 2011; Katzner et al., 2009; Kreiman et al., 2006; Łęski et al., 2013; Liu and Newsome, 2006; Rogers et al., 2019; Xing et al., 2009). Macro-scale clinical electrodes may mask spatially fine sub-millimeter scale LFP signals as broader synchronization would be required to effect change in the summed potential of larger neuronal populations integrated by the larger electrodes (Kellis et al., 2016; Rogers et al., 2019). The action potential (AP)-aligned average LFP, or spike-triggered average LFP, has been used to characterize the functional relationship between individual neurons and LFP (Nauhaus et al., 2009; Okun et al., 2010; Ray and Maunsell, 2011).

The aim of this study was to characterize the neural activity in subcortical and cortical regions involved in the mechanism of DBS on the micro- to mesoscale without applying any stimulation. Our hypothesis was that neuron firing in the STN used as a target for DBS therapy would be significantly connected to activity in the motor association cortex in a pattern that displayed differences on a sub centimeter scale. This work displays the variety and specificity of subcortical-cortical relationships and our need to understand cortical microcircuits involved in PD and DBS. Furthering our knowledge of the cortico-basal ganglia circuit in PD will lead to advances in understanding the pathophysiology of PD and in novel treatment strategies. There has been much attention paid to the time and frequency aspects of neural rhythms in PD (e.g. beta, gamma), particularly in connection with DBS. In addition to these temporal aspects of LFP, we point out the importance of the spatial organization of neural rhythms. This study examined a spatial topography on a sub-centimeter scale in order to inspect the cortico-basal ganglia circuit with a high degree of spatial resolution. We anticipate that work in this realm will lead to the generation of potential biomarkers of PD symptoms that may be used for responsive stimulation or better targeting of neuromodulation therapies.

2. Methods

2.1. Subjects

Experimental subjects were volunteer patients with PD undergoing standard anesthetized bilateral DBS implant surgery at Barrow Neurological Institute in St. Joseph's Hospital (Phoenix, AZ). Potential candidates were evaluated by a multidisciplinary team, including a fellowship-trained movement disorders neurologist, neuropsychologist, and neurosurgeon. Patients were considered appropriate for DBS if they had a diagnosis of idiopathic PD with 1) an adequate response to dopaminergic medication (assessed using the Unified Parkinson's Disease Rating Scale to compare the on-medication state to the off-medication state) and 2) disabling motor fluctuations, dyskinesia, or severe functional impairment despite medical management. Demographic information is included in Table 1. All patients consented to participate in this study, and the methods were reviewed and approved by the Institutional Review Board (IRB) at St. Joseph's Hospital.

2.2. Equipment and recording setup

DBS electrodes were placed bilaterally following standard surgical procedure using frame-based stereotaxy (Leksell G frame, Elekta Instrument AB, Stockholm, Sweden) in anesthetized patients (Chen et al., 2018; Mirzadeh et al., 2014). Stereotactic planning for each subject was performed on a S8 Stealth Station (Medtronic). Patients were allowed to take their PD medications on the morning of surgery. The STN target was initially set using Talairach coordinates (±12, −2, 0) and then adjusted based upon direct anatomical visualization using T2-weighted magnetic resonance imaging (MRI) sequences (2-mm slices; 3-T MRI, General Electric; see Supplemental Fig. 2). Trajectories were planned initially at 60 degrees

Table 1
Patient Demographics.

Subject	Age	Sex	Target	DBS Implant	Years of PD	Recorded Hemisphere
1	62	M	STN	Bilateral	4	Right
2	65	M	STN	Bilateral	12	Left
3	65	F	STN	Bilateral	10	Right
4	65	M	STN	Bilateral	6	Right
5	67	M	STN	Bilateral	6	Right
6	55	M	STN	Bilateral	7	Right

Abbreviations: M, male; F, female; STN, subthalamic nucleus; DBS, deep brain stimulation; PD, Parkinson's disease.

from the axial plane and 20 degrees from the mid-sagittal plane and adjusted to be at least 4 mm from the ventricle and to avoid sulci and blood vessels. The stereotactic frame was placed immediately after induction of general anesthesia and high-resolution thin slice computerized tomography (CT) images were obtained intraoperatively for confirmation of the DBS lead at the target (BodyTom mobile CT scanner, Neurologica Corp). During the recording period only propofol was used for anesthesia, except the first subject, when a trial was done for recording with propofol versus dexmedetomidine. On the non-dominant hemisphere (right for 5/6 subjects, left for 1/6 subjects), a 4 contact by 4 contact micro-ECoG array (2 mm spacing and 75 um diameters; impedance range: 90–370 MΩ; PMT Neurosurgical, Chanhassen, MN) was placed epicortically on motor association cortex (Fig. 1) at Talairach coordinates (19.75, 9.25, 66). A subcortical microelectrode (FHC, Bowdoin, ME) was inserted through a cannula in the same burr hole used for DBS electrode placement (Fig. 1, the DBS lead is shown as an illustration of our recording set up, though in this study we did not perform any stimulation, nor did we record any LFP from the DBS lead). Simultaneous recordings from the epicortical micro-ECoG grid and the subcortical microelectrode were sampled at 24.4 kHz with a data acquisition system (Tucker-Davis Technologies, Alachua, FL). Recording was continuous, and as the microelectrode was lowered, we stopped at multiple sites with neuronal activity for periods of approximately 0.5–5 minutes. The STN was identified based on stereotaxic coordinates and characteristic firing patterns. After research recordings were completed, the microelectrode and micro-ECoG grid were removed, and surgery was completed using standard procedure.

2.3. Analysis

All analysis was completed in MATLAB (The MathWorks, Inc., Natick, MA). For neuron spike isolation, data was band pass filtered with a 2nd order elliptical filter from 300-3000 Hz. Spike-sorting was performed using wavelets and a superparamagnetic clustering algorithm (Chaure et al., 2018; Quian Quiroga et al., 2004). Single-unit neurons were isolated based on criteria of firing for at least 30 seconds, a total of at least 200 APs recorded, the shape of the histogram of inter-AP timing [the inter-spike interval (ISI)], and visual inspection (authors BG and AG). Firing rate was calculated in 2 second bins. For LFP analysis, data was low pass filtered with a 3rd order elliptical filter with a cutoff frequency of 250 Hz and a comb filter for 60 Hz noise. The broadband LFP (0–250 Hz) was examined in this study to refrain from bias towards a specific frequency band. For each isolated subcortical neuron and at each location (one in the STN and 16 in the cortex for a sum of 17 locations for each neuron), the LFP data from the cortical micro-ECoG and the subcortical microelectrode were extracted from −1 sec to + 1 sec about individual AP times with each AP time set to 0 sec. These data snippets were averaged to generate AP-aligned average LFP waveforms (also known as the spike-triggered average). Control data were resampled from the filtered LFP waveform by jittering all the spike times for that individual neuron randomly from −1 to 1 seconds with uniform probability. For each neuron and at each location, the 99.7 % confidence intervals for the AP-aligned average LFP and the jittered AP-aligned average LFP (control data) were calculated using the all of the APs for that neuron and the respective LFP snippets at each location temporally surrounding the APs from −1 sec to + 1 sec about individual AP times. A location was determined to have statistical significance if the 99.7 % confidence intervals for the AP and jittered-AP aligned LFPs did not overlap for more than 6 ms out of the 2 second window (which equates to the 0.3 % false positive rate of hypothesis testing by nonoverlapping 99.7 % confidence intervals). The same APs from the STN neurons were used to generate the AP-aligned average LFP in both the STN and the cortex (16 channels/electrode grid locations). The open-source Chronux library for Matlab (https://chronux.org/; Mitra and Bokil, 2008) was used for spike-field phase analysis, where a sinusoidal function at 4 Hz was fit to the AP-aligned average LFP and the phase at time 0 represents the phase of the average LFP when the AP occurs.

3. Results

We recorded neural data from 6 subjects in 44 locations in the STN [average number of STN locations per patient: 7.3 (±1.1); time spent in one STN location: average 2.1 minutes, range 0.5–7.1 minutes). 65 putative AP clusters were identified, and a final set of 46 neurons was included in the analysis [average number of neurons identified per patient: 7.5 (±1.5); Fig. 2A,B, see also Table 2]. The average firing rate was 21.9 ± 2.2 Hz (Fig. 2C). Histograms of inter-AP times (ISI) showed right skewed distributions with peaks in the 3–18 ms range for 41/46 cells. 5 cells had ISI histograms with peaks at later times due to slower firing rates (Fig. 2D).

The AP-aligned average LFP (i.e. spike-triggered average) between APs from a single STN neuron and the LFP in the STN was significant (nonoverlapping 99.7 % confidence intervals) for 18/46 (39.1 %) neurons (Fig. 3A; example of a non-significant STN neuron in Fig. 3B; see also Supplemental Fig. 1). LFP power was highest in frequencies below 12 Hz (Fig. 3C), with the delta band (0.5–4 Hz) dominating, and some power seen in the alpha band (8–12 Hz). When the LFP at a frequency of 4 Hz was examined for the phase at which the spike occurred, the phase varied widely for STN neurons with both significant or non-significant AP-aligned average LFP (Fig. 3D). In summary, STN neuron APs and their relationship to the STN LFP did not show a consistent phase relationship to the LFP across neurons. Some STN neurons exhibited a significant relationship with the local field, though not at any particular LFP phase, and other neurons did not show any significant functional connectivity.

Next, the cortical LFP was examined for its relationship to the STN neurons. 25/46 (54.3 %) STN neurons exhibited a significant functional relationship with at least one location on the cortex, with several having significant relationships at more than one location (Fig. 4A,B). LFP power in the cortex was similar to LFP power in the STN, with power highest in frequencies below 12 Hz (Fig. 4C; see also Supplemental Fig. 1). Again similar to our observations

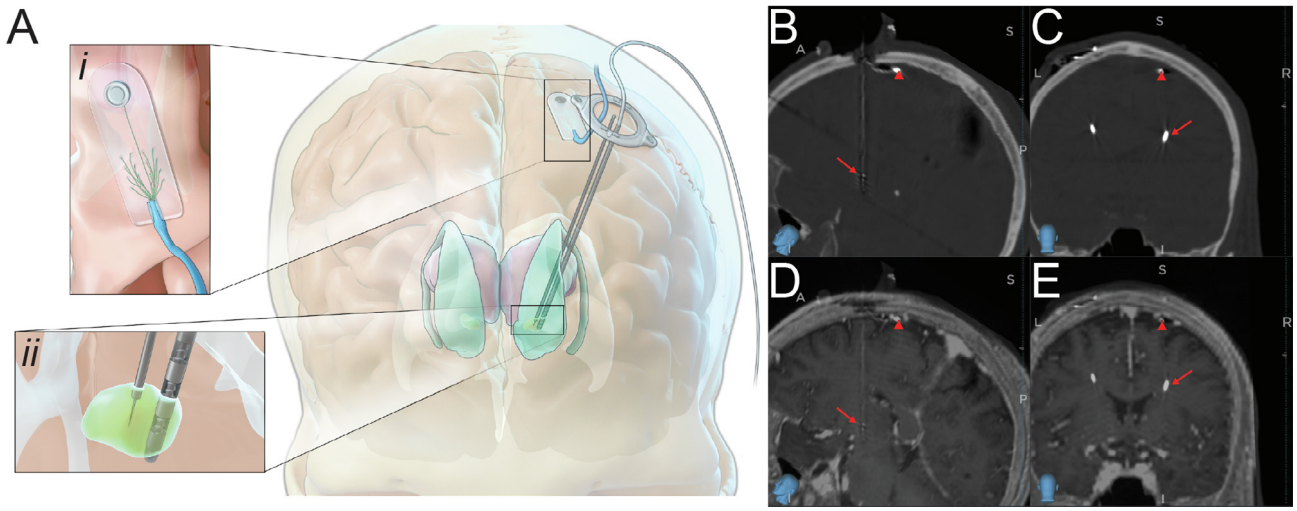

Fig. 1. Intraoperative recording electrode setup. (A) Illustration of recording set up with a coronal view of the head. Inset *i* shows the epicortical micro-ECoG grid which records LFPs on each of its 16 channels with electrodes placed 2 mm from each other and a reference electrode. Inset *ii* shows the microelectrode which is placed in the STN adjacent to the DBS electrode and records APs and LFPs. The DBS lead is shown as an illustration of our recording set up, though in this study we did not include any stimulation. Please note that all recordings in the STN were from the microelectrode, and not the DBS lead. (B,C) Intraoperative CT image and (D,E) co-registered preoperative MRI and intraoperative CT images showing the DBS electrode (red arrow, positioned at Talairach coordinates [12.4, −1.8, −4]) and the micro-ECoG grid with reference electrode (red triangle, positioned at Talairach coordinates [19.75, 9.25, 66]). View is displayed in the bottom left corner by the illustration of a blue head. Anatomical directions are given by A (anterior), P (posterior), S (superior), I (inferior), R (right) and L (left). Abbreviations: micro-ECoG, microelectrocorticography; LFP, local field potential; STN, subthalamic nucleus; DBS, deep brain stimulation; AP, action potential; CT, computed tomography; MRI, magnetic resonance imaging.

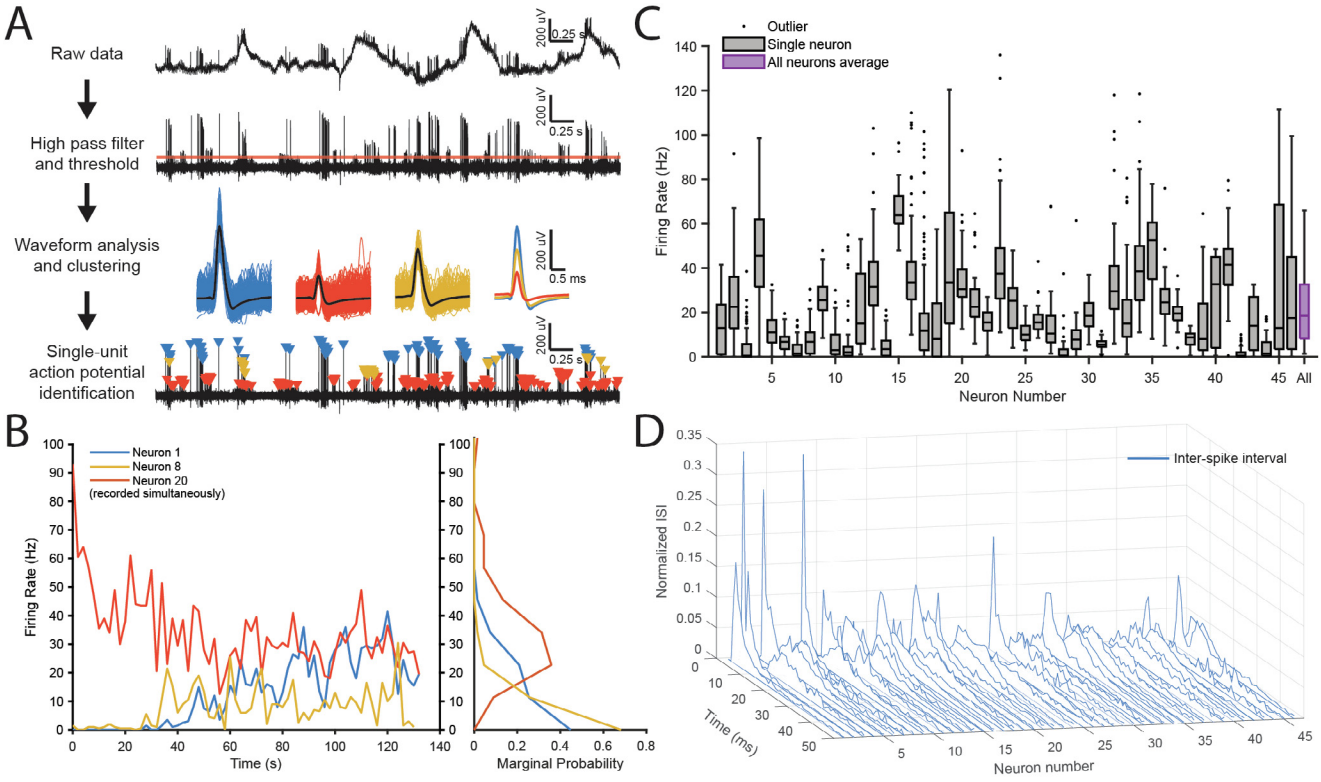

Fig. 2. Spike sorting and STN neuron properties. (A) Workflow for offline AP isolation and spike sorting. A recording with 3 example STN neurons (blue, red, yellow traces and triangle markers) is shown. Scale bars are shown on the right side of each trace. (B) Firing rate of 3 example STN neurons (blue, red, yellow) that were recorded simultaneously (the same neurons as in A). (C) Boxplots of firing rate for all 46 STN neurons in this study. (D) Inter-spike interval (ISI) for all 46 STN neurons in this study. Abbreviations: STN, subthalamic nucleus; AP, action potential; ISI, inter-spike interval.

in the STN LFP, the phase of the 4 Hz LFP in the cortex when the spike occurs varied widely, with no distinct pattern for cortical locations with or without a significant spike-field relationship (Fig. 4D).

Importantly, STN neurons recorded simultaneously (presumably located within a few hundred micrometers) did not display the same spatial pattern of functional connectivity with the cortex (Fig. 5; examples in Fig. 4A,B and Supplemental Fig. 1). Neurons

Table 2
STN neuron characteristics.

Number of STN neurons isolated	46
Recording locations with 1 isolated neuron	25
Recording locations with 2 isolated neurons	6
Recording locations with 3 isolated neurons	3
Average firing rate (±standard error)	21.9 (±2.2) Hz
Average number of action potentials identified for one neuron (±standard error)	2381.2 (±306.5)
Number of neurons with significant relationship to LFP in STN (nonoverlapping 99.7 % confidence intervals)	18 (39.1 %)
Number of neurons with significant relationship to LFP in ≥ 1 cortical channels (nonoverlapping 99.7 % confidence intervals)	25 (54.3 %)
Number of neurons with significant relationship to LFP in both STN and ≥ 1 cortical channels (nonoverlapping 99.7 % confidence intervals)	10 (21.7 %)

Abbreviations: STN, subthalamic nucleus; LFP, local field potential.

that were recorded at the same time and location did not have identical relationships either in the STN or at the various cortical locations (Fig. 5, see superscript letters for neurons recorded simultaneously). In summary, 18/46 (39.1 %) STN neurons showed significant functional connectivity with the STN LFP, and 25/46 (54.3 %) STN neurons showed significant functional connectivity with the cortex. The area of motor association cortex observed has a non-uniform spatial topography of significant connectivity with STN neurons that sometimes differed between adjacent locations 2 mm apart (Fig. 5). 10/46 (21.7 %) STN neurons had significant AP-aligned average LFPs in both the STN LFP and at least one location on the cortex (Table 2).

4. Discussion

The objective of this study was to examine the electrophysiological relationships within the cortico-basal ganglia circuit on a sub-centimeter scale. We found a complex spatial topography of electrophysiological functional connections between single STN neurons, the LFP in the STN, and the LFP in the motor association cortex that exists on a sub-centimeter scale (i.e. a high spatial specificity). We placed a priority on identifying single STN neurons and examining the cortex with a micro-ECoG grid in order to characterize this circuit on a spatial scale relevant to the spatial scale of cortical columns in the human brain. The neurons that displayed a

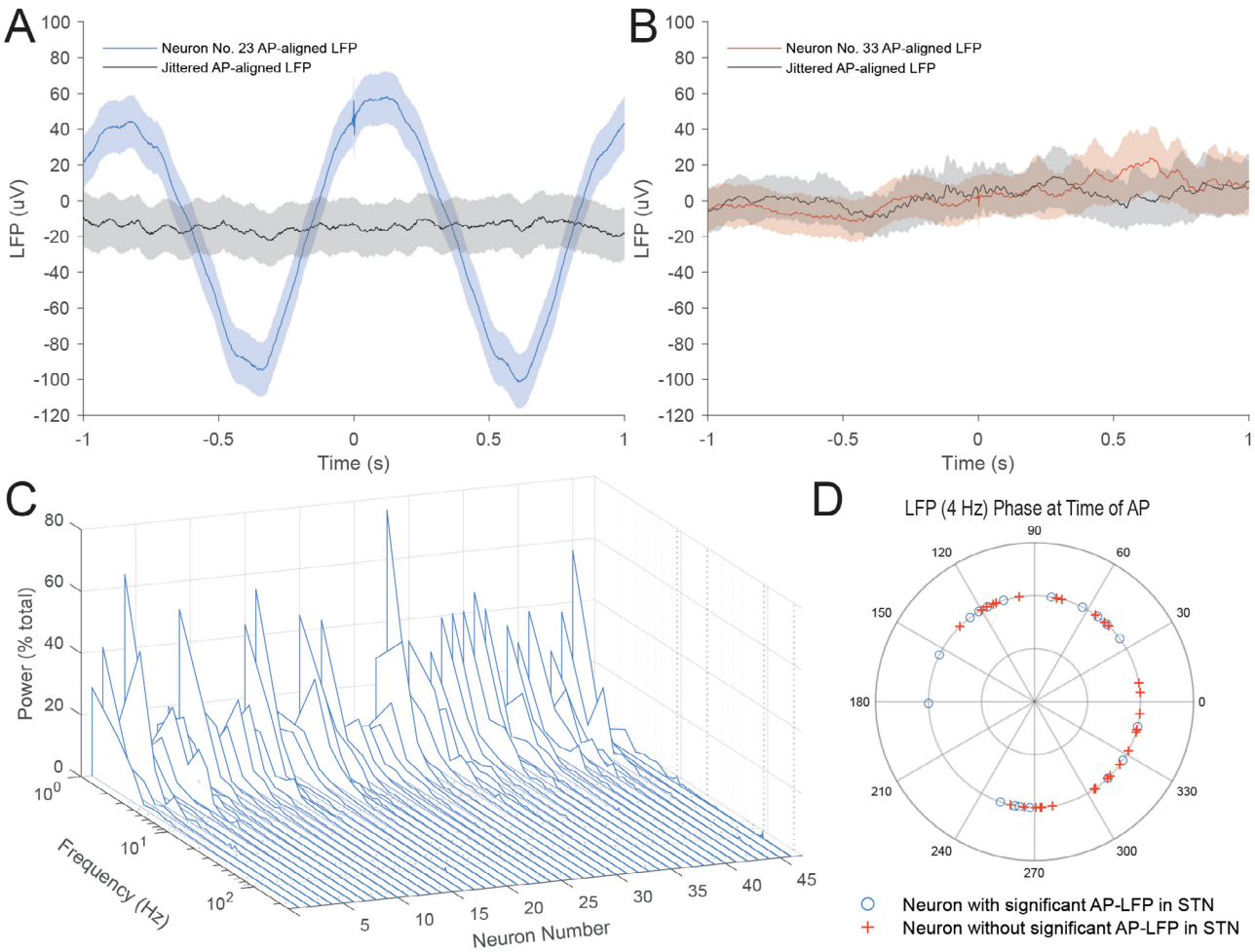

Fig. 3. STN neuron AP-aligned average LFP in STN. (A,B) Representative examples of STN neurons with (A, blue trace) and without (B, red trace) a significant relationship (non-overlapping 99.7 % confidence intervals) between the neuron spike and the AP-aligned average LFP in the STN. Control data (black trace) is aligned on the jittered APs (randomly from −1 to + 1 s). Shading around each trace represents the 99.7 % confidence interval. (C) Power spectrums of AP-aligned average LFP for all 46 neurons recorded. (D) Phase of spike relative to the STN LFP measured at 4 Hz for all 46 neurons recorded. Additional data are included in Supplemental Fig. 1. Abbreviations: STN, subthalamic nucleus; AP, action potential; LFP, local field potential.

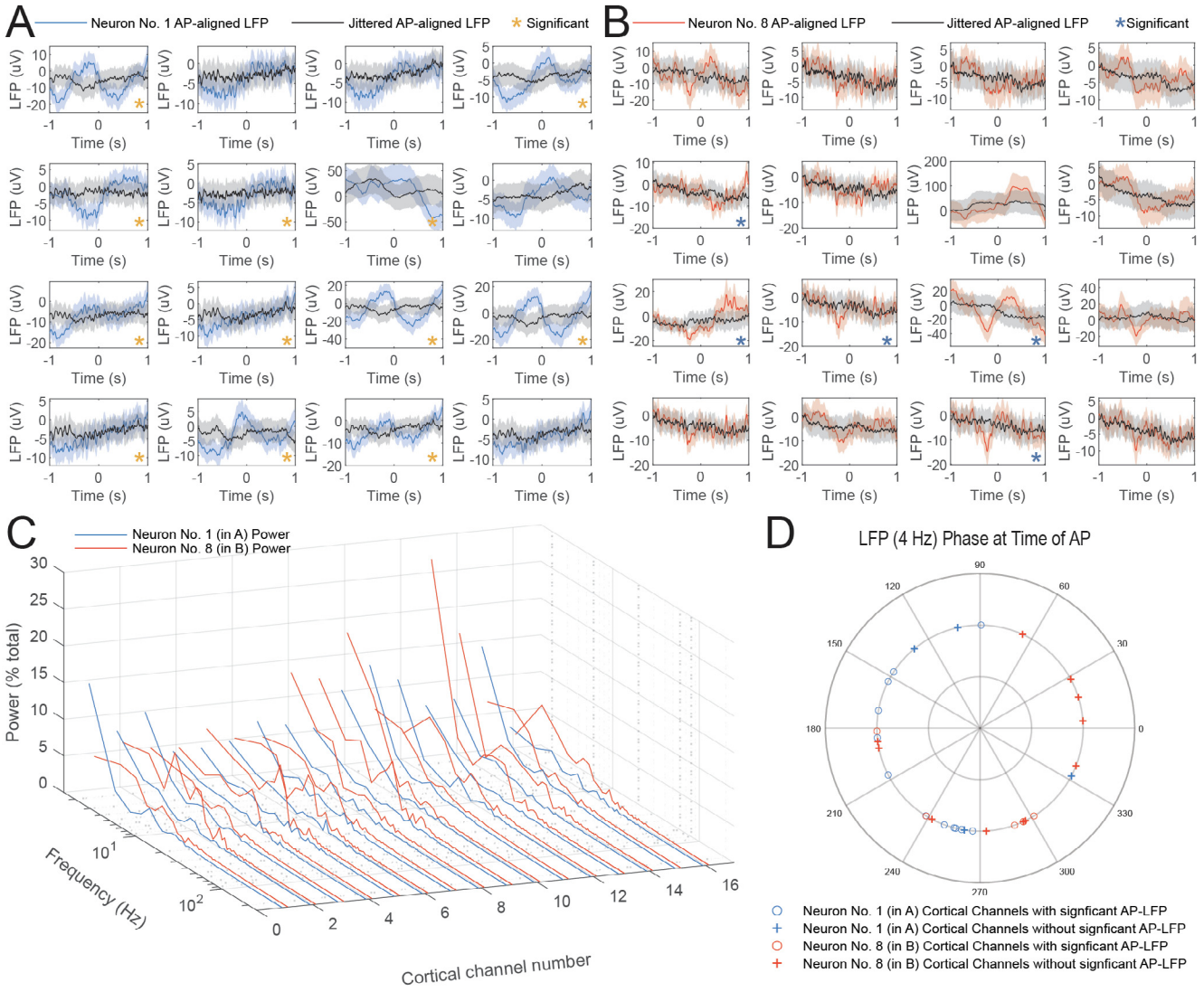

Fig. 4. STN neuron AP-aligned average LFP in cortex. (A,B) Two representative examples (blue trace and red trace, respectively) of average LFP recordings from the epicortical 4 × 4 channel micro-ECoG grid aligned on APs from two individual STN neurons that were recorded simultaneously, and are presumably neighboring neurons. Control data (black trace) is aligned on the jittered APs (randomly from −1 to + 1 s). Shading around each trace represents the 99.7 % confidence interval. Locations (channels) that have a significant electrophysiological functional relationship (non-overlapping 99.7 % confidence intervals) are marked with an asterisk. (C) Power of the STN neuron AP-aligned average cortical LFP for each of the 16 channels for the two STN neurons shown in A and B. (D) Phase of the spike at 4 Hz for each of the 16 channels for the two STN neurons shown in A and B. Additional data are included in Supplemental Fig. 1. Abbreviations: STN, subthalamic nucleus; AP, action potential; LFP, local field potential; micro-ECoG, microelectrocorticography.

functional connection to the cortex have sub-centimeter spatial differences on the cortex and between individual neurons. This single neuron and sub-centimeter spatial specificity was essential to examine small micro- to meso-circuits within the greater cortico-basal ganglia circuit. STN neurons from the same recording (presumably within a few hundred microns from each other) did not display the same functional connectivity topography on the cortical region recorded. The relatively small area of cortex recorded in this study shows differing relationships to the STN, sometimes only 2 mm apart. It is plausible that if we were to look at a larger area of the cortex with the same spatial resolution, we would find that STN neurons continue to exhibit unique functional connectivity topographies, and that some neurons where we found no cortical functional connections would indeed be electrophysiologically linked to areas of the cortex outside of our recording region. These topographical patterns are interesting because they show that neurons in the cortico-basal ganglia network are not uniformly connected. Our results showed that within the context of larger anatomical connections of the cortico-basal ganglia network, there are embedded smaller meso- or micro-scale circuits involving subsets of neurons and dendritic arbors.

This study exemplified the utility of micro-ECoG devices and recordings for research purposes. Our results showed differing relationships on the cortex with neurons in the STN using a micro-ECoG grid with 2 mm electrode spacing. We advocate for the use of micro-ECoG electrodes and other devices designed to look at the cortex on a sub-centimeter scale, especially as these devices are developed for AP recordings without penetrating electrodes (Khodagholy et al., 2015). We should recognize the utility of examining the cortex on a scale relevant to the circuit organization with micro-ECoGs in applicable research studies.

We found many of our effects in low frequency bands of LFP, like delta, theta, and alpha. We did not see a consistent phase relationship between APs and LFP in either the STN or the cortex for neurons with significant functional connectivity. Across neurons, the AP occurred at a variety of LFP phases including both the peak

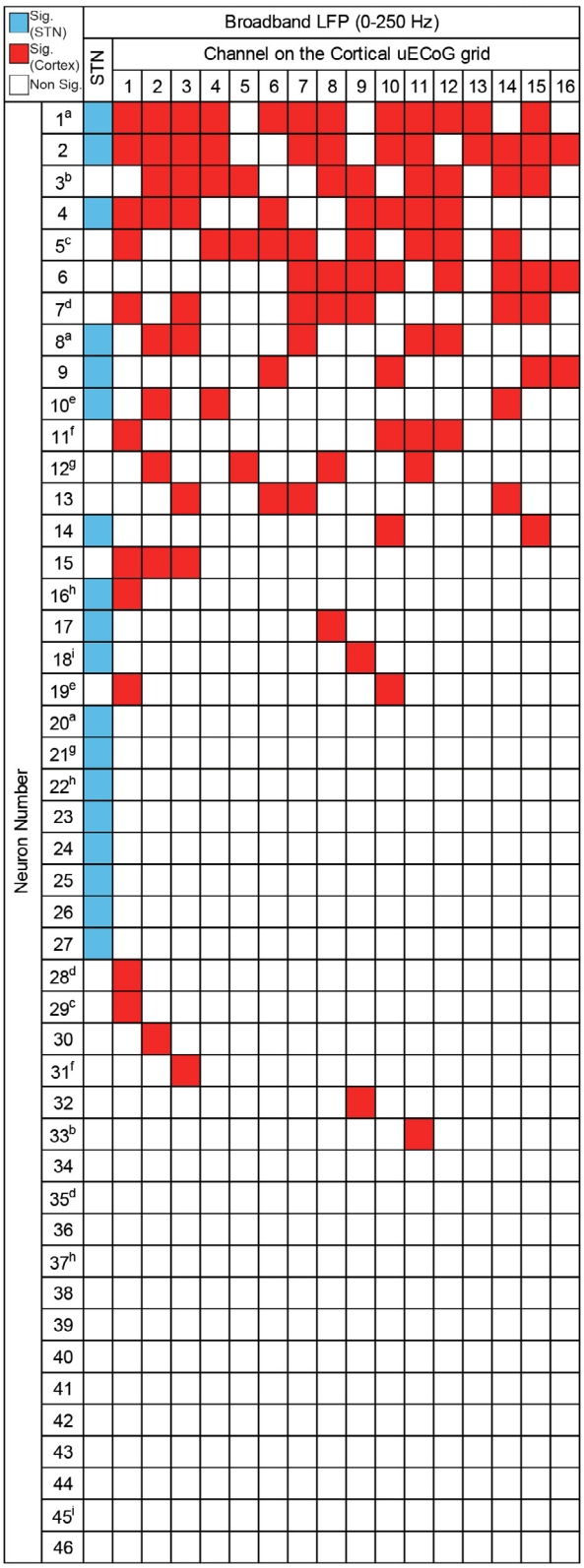

Fig. 5. Summary of STN neuron to STN LFP and cortical LFP functional connectivity. Connections for all recorded neurons to both the STN and every cortical channel are shown, with boxes filled in when the AP-aligned LFP for that relationship is statistically significant (non-overlapping 99.7% confidence intervals). Blue represents the STN and red represents the cortex. Neurons recorded at the same location and time (assumed near-neighbors) are marked with the same superscript letters a-i. Abbreviations: STN, subthalamic nucleus; LFP, local field potential; AP, action potential; Sig., statistically significant; uECoG, microelectrocorticography.

and the trough. The diverse LFP phases at which the AP of different neurons occur result in no statistically significant findings in phase, but do give interesting insight into the electrophysiological heterogeneity of the STN and STN-cortical functional connections. These results suggest that neurons in the STN are not uniformly entrained to the same LFP frequency, regardless of if that LFP is generated locally or from an input to the STN. For example, a local STN neuron could be significantly connected to the STN LFP, and a projection STN neuron could be significantly connected to the cortical LFP, and some neurons may be tuned in to both distant and local LFP. These findings may correlate to distinct subpopulations of STN neurons and their contributions to the overall cortico-BG circuit, but more research is needed to understand the role of the individual STN neuron embedded in the network.

We are interested in how various LFP frequencies may give rise to symptoms of PD, especially those symptoms that are not targeted well by DBS. The link between beta rhythms in the STN LFP and bradykinesia seems clear (Tinkhauser et al., 2017; Whitmer et al., 2012), but growing evidence points to a need to examine other LFP rhythms as well, either because beta hypersynchrony alone is insufficient, or because of a link between other neural rhythms and PD symptoms (Devergnas et al., 2014; Heinrichs-Graham et al., 2014; Quiroga-Varela et al., 2013; Swan et al., 2019; Zhang et al., 2018). Theta LFP rhythms may contribute to tremor (Asch et al., 2020), and gamma LFP rhythms, particularly in the cortex (de Hemptinne et al., 2015; Swann et al., 2018), may mediate motor symptoms such as tremor or dyskinesia. Motor symptoms that evade DBS therapy may be modulated through frequencies other than beta. To improve DBS for PD, we need to find how beta hypersynchrony interacts with other electrophysiological functions. We cannot treat beta rhythms as spatially ubiquitous in the STN (Zhang et al., 2018), and we must look at how other frequencies influence the motor symptoms of PD. We encourage investigation into lower frequencies because of our data here, as well as higher frequencies that we were unable to observe in this study.

Several of the weaknesses of this study revolve around the constraints of human subjects research, which calls for a high priority on the safety of the subjects, closely followed by a priority on care for optimizing the clinical outcomes for the subjects. Thus, limitations include a small sample size of human subjects, limited recording time in the intraoperative setting (unable to let neuron firing stabilize for longer than a few seconds), the use of anesthesia during recordings, and limited access to the cortex. Patients were recruited consecutively, but we have a bias towards males in our sample, which can only be partially explained by a predominance of PD in men versus women (Ascherio and Schwarzschild, 2016). The patients recruited represent a subset of all patients with PD that have a tremor-predominant phenotype and a good response to levodopa. The use of propofol anesthesia is a concerning confound because of the effect of propofol to decrease APs and high-frequency LFPs (Brown et al., 2011; Hanrahan et al., 2013), which may explain in part why we saw effects predominantly at low frequencies. We acknowledge this concern but point out that our findings show microcircuit interactions even with the influence of anesthesia. Additionally, this study is conducted entirely in the context of Parkinson's disease, and so any extrapolation to learning the function of the healthy brain is constrained. Because of surgical constraints, we had limited spatial access to the cortex, which lent to variation between the exact placement of the micro-ECoG between patients. Factors such as variable contact between electrodes and the cortical surface, interfering vasculature or sulci, and other anatomical variation were challenging to control in an intraoperative setting.

Follow up research to this study includes two main branches: understanding the mechanism of DBS and understanding

cortical-subcortical functional relationships. We are presently examining the same functional relationships studied here with the addition of intraoperative DBS. Additionally, we would like to repeat these studies in awake patients, both intraoperatively and post operatively, which would provide greater insight to higher frequencies of LFPs involved in this cortico-basal ganglia microcircuit. We speculate that the functional connectivity seen in this study would be even more robust in awake patients and may even show some correlation with PD symptoms. DBS technology has advanced to allow for recording field potentials in settings outside the operating room or the clinic. As we further investigate neural networks involved with DBS, we will be able to generate potential biomarkers for adaptive DBS, learn how to target directional DBS, and improve the therapy in movement disorders for both motor symptoms and other symptoms that have been more difficult to treat. For other applications of DBS, we hope that continuing to pursue knowledge about how DBS affects neurons and neural tissue on a fundamental level will inform targeting and programing for other brain disorders (Lee et al., 2019; Lozano et al., 2019). Additionally, future directions of this research include further characterization of motor information processing in the cortico-basal ganglia network in both the impaired and healthy brains. As we understand more about both the temporal and spatial dynamics of LFP frequencies in the cortico-basal ganglia network, we will be more equipped to target therapies for PD in a more specific manner.

5. Conclusions

The STN and the motor association cortex had an intricate and complex functional connectivity with a high degree of spatial specificity. Individual neurons in the STN showed electrophysiological functional connectivity with the LFP, both locally (STN) and at a distance (motor association cortex). The topographies of these functional connections varied across neurons and on a subcentimeter scale on the cortex. Examining the cortico-basal ganglia circuit is important in the effort to understand both normal and abnormal motor information processing and to improve neuromodulation therapies.

Declaration of Competing Interest

The authors declare that they have no known competing financial interests or personal relationships that could have appeared to influence the work reported in this paper.

Acknowledgements

The authors are grateful for the participation of the patients who were subjects in this study. We would also like to thank Meg Lambert and the staff at Barrow Neurological Institute for their assistance in recruiting, managing, and caring for the patients in this study. Financial support for this project came from the SK Foundation and the Barrow Center for Neuromodulation. We also want to thank the Biostatistics and Study Design Services at the University of Arizona College of Medicine—Phoenix for their consults on statistical analysis for this study.

Appendix A. Supplementary data

Supplementary data to this article can be found online at https://doi.org/10.1016/j.clinph.2022.06.017.

References

Albin RL, Young AB, Penney JB. The functional anatomy of disorders of the basal ganglia. Trends Neurosci 1995;18:63–4. https://doi.org/10.1016/0166-2236(95)80020-3.

Amadeus Steiner L, Barreda Tomás FJ, Planert H, Alle H, Vida I, Geiger JRP. Connectivity and Dynamics Underlying Synaptic Control of the Subthalamic Nucleus. J Neurosci 2019;39:2470. https://doi.org/10.1523/JNEUROSCI.1642-18.2019.

Asch N, Herschman Y, Maoz R, Auerbach-Asch CR, Valsky D, Abu-Snineh M, et al. Independently together: subthalamic theta and beta opposite roles in predicting Parkinson's tremor. Brain Commun 2020;2. https://doi.org/10.1093/BRAINCOMMS/FCAA074.

Ascherio A, Schwarzschild MA. The epidemiology of Parkinson's disease: risk factors and prevention. Lancet Neurol 2016;15:1257–72.

Berens P, Keliris GA, Ecker AS, Logothetis NK, Tolias AS. Feature Selectivity of the Gamma-Band of the Local Field Potential in Primate Primary Visual Cortex. Front Neurosci 2008;2:199. https://doi.org/10.3389/NEURO.01.037.2008.

Brown EN, Purdon PL, Van Dort CJ. General Anesthesia and Altered States of Arousal: A Systems Neuroscience Analysis. Annu Rev Neurosci 2011;34(1):601–28.

Buzsáki G, Anastassiou CA, Koch C. The origin of extracellular fields and currents — EEG, ECoG. LFP and spikes Nat Rev Neurosci 2012;13(6):407–20.

Cagnan H, Duff EP, Brown P. The relative phases of basal ganglia activities dynamically shape effective connectivity in Parkinson's disease. Brain 2015;138(6):1667–78.

Chaure FJ, Rey HG, Quian QR. A novel and fully automatic spike-sorting implementation with variable number of features. J Neurophysiol 2018;120:1859–71. https://doi.org/10.1152/jn.00339.2018 [doi].

Chen T, Mirzadeh Z, Chapple KM, Lambert M, Shill HA, Moguel-Cobos G, Tröster AI, Dhall R, Ponce FA. Clinical outcomes following awake and asleep deep brain stimulation for Parkinson disease. J Neurosurg 2018;130(1):109–20.

Cole SR, van der Meij R, Peterson EJ, de Hemptinne C, Starr PA, Voytek B. Nonsinusoidal Beta Oscillations Reflect Cortical Pathophysiology in Parkinson's Disease. J Neurosci 2017;37(18):4830–40.

Deuschl G, Schade-Brittinger C, Krack P, Volkmann J, Schäfer H, Bötzel K, Daniels C, Deutschländer A, Dillmann U, Eisner W, Gruber D, Hamel W, Herzog J, Hilker R, Klebe S, Kloß M, Koy J, Krause M, Kupsch A, Lorenz D, Lorenzl S, Mehdorn HM, Moringlane JR, Oertel W, Pinsker MO, Reichmann H, Reuß A, Schneider G-H, Schnitzler A, Steude U, Sturm V, Timmermann L, Tronnier V, Trottenberg T, Wojtecki L, Wolf E, Poewe W, Voges J. A Randomized Trial of Deep-Brain Stimulation for Parkinson's Disease. N Engl J Med 2006;355(9):896–908.

Devergnas A, Pittard D, Bliwise D, Wichmann T. Relationship between oscillatory activity in the cortico-basal ganglia network and parkinsonism in MPTP-treated monkeys. Neurobiol Dis 2014;68:156. https://doi.org/10.1016/J.NBD.2014.04.004.

Eisinger RS, Cernera S, Gittis A, Gunduz A, Okun MS. A review of basal ganglia circuits and physiology: application to deep brain stimulation. Parkinsonism Relat Disord 2019;59:9. https://doi.org/10.1016/J.PARKRELDIS.2019.01.009.

Engel AK, König P, Gray CM, Singer W. Stimulus-Dependent Neuronal Oscillations in Cat Visual Cortex: Inter-Columnar Interaction as Determined by Cross-Correlation Analysis. Eur J Neurosci 1990;2:588–606. https://doi.org/10.1111/J.1460-9568.1990.TB00449.X.

Farokhniaee A, Lowery MM. Cortical network effects of subthalamic deep brain stimulation in a thalamo-cortical microcircuit model. J Neural Eng 2021;18. https://doi.org/10.1088/1741-2552/ABEE50.

Group TD-BS for PDS. Deep-Brain Stimulation of the Subthalamic Nucleus or the Pars Interna of the Globus Pallidus in Parkinson's Disease. N Engl J Med 2001;345:956–63. https://doi.org/10.1056/NEJMoa000827.

Hanrahan SJ, Greger B, Parker RA, Ogura T, Obara S, Egan TD, et al. The effects of propofol]on local field potential spectra, action potential firing rate, and their temporal relationship in humans and felines. Front Hum Neurosci 2013:1–26. https://doi.org/10.3389/FNHUM.2013.00136/BIBTEX.

Heinrichs-Graham E, Kurz MJ, Becker KM, Santamaria PM, Gendelman HE, Wilson TW. Hypersynchrony despite pathologically reduced beta oscillations in patients with Parkinson's disease: A pharmaco-magnetoencephalography study. J Neurophysiol 2014;112:1739–47. https://doi.org/10.1152/JN.00383.2014/ASSET/IMAGES/LARGE/Z9K0191426280004.JPEG.

de Hemptinne C, Swann NC, Ostrem JL, Ryapolova-Webb ES, San Luciano M, Galifianakis NB, Starr PA. Therapeutic deep brain stimulation reduces cortical phase-amplitude coupling in Parkinson's disease. Nat Neurosci 2015;18(5):779–86.

Herrington TM, Cheng JJ, Eskandar EN. Mechanisms of deep brain stimulation. J Neurophysiol 2016;115:19–38. https://doi.org/10.1152/JN.00281.2015.

Jia X, Smith MA, Kohn A. Stimulus Selectivity and Spatial Coherence of Gamma Components of the Local Field Potential. J Neurosci 2011;31(25):9390–403.

Katzner S, Nauhaus I, Benucci A, Bonin V, Ringach DL, Carandini M. Local origin of field potentials in visual cortex. Neuron 2009;61(1):35–41.

Kellis S, Sorensen L, Darvas F, Sayres C, O'Neill K, Brown RB, House P, Ojemann J, Greger B. Multi-scale analysis of neural activity in humans: Implications for micro-scale electrocorticography. Clin Neurophysiol 2016;127(1):591–601.

Khodagholy D, Gelinas JN, Thesen T, Doyle W, Devinsky O, Malliaras GG, Buzsáki G. NeuroGrid: recording action potentials from the surface of the brain. Nat Neurosci 2015;18(2):310–5.

Kreiman G, Hung CP, Kraskov A, Quiroga RQ, Poggio T, DiCarlo JJ. Object Selectivity of Local Field Potentials and Spikes in the Macaque Inferior Temporal Cortex. Neuron 2006;49:433–45. https://doi.org/10.1016/J.NEURON.2005.12.019.

Krimer LS, Goldman-Rakic PS. Prefrontal Microcircuits: Membrane Properties and Excitatory Input of Local, Medium, and Wide Arbor Interneurons. J Neurosci 2001;21(11):3788–96.

Kühn AA, Trottenberg T, Kivi A, Kupsch A, Schneider GH, Brown P. The relationship between local field potential and neuronal discharge in the subthalamic nucleus of patients with Parkinson's disease. Exp Neurol 2005;194:212–20. https://doi.org/10.1016/J.EXPNEUROL.2005.02.010.

Lee DJ, Lozano CS, Dallapiazza RF, Lozano AM. Current and future directions of deep brain stimulation for neurological and psychiatric disorders. J Neurosurg 2019;131:333–42.

Łęski S, Lindén H, Tetzlaff T, Pettersen KH, Einevoll GT, Sporns O. Frequency Dependence of Signal Power and Spatial Reach of the Local Field Potential. PLoS Comput Biol 2013;9(7):e1003137.

Liu J, Newsome WT. Local Field Potential in Cortical Area MT: Stimulus Tuning and Behavioral Correlations. J Neurosci 2006;26(30):7779–90.

Lopez-Azcarate J, Tainta M, Rodriguez-Oroz MC, Valencia M, Gonzalez R, Guridi J, Iriarte J, Obeso JA, Artieda J, Alegre M. Coupling between Beta and High-Frequency Activity in the Human Subthalamic Nucleus May Be a Pathophysiological Mechanism in Parkinson's Disease. J Neurosci 2010;30(19):6667–77.

Lozano AM, Lipsman N, Bergman H, Brown P, Chabardes S, Chang JW, Matthews K, McIntyre CC, Schlaepfer TE, Schulder M, Temel Y, Volkmann J, Krauss JK. Deep brain stimulation: current challenges and future directions. Nat Rev Neurol 2019;15(3):148–60.

McColgan P, Joubert J, Tabrizi SJ, Rees G. The human motor cortex microcircuit: insights for neurodegenerative disease. Nat Rev Neurosci 2020;21:401–15. https://doi.org/10.1038/s41583-020-0315-1.

Miocinovic S, de Hemptinne C, Chen W, Isbaine F, Willie JT, Ostrem JL, Starr PA. Cortical Potentials Evoked by Subthalamic Stimulation Demonstrate a Short Latency Hyperdirect Pathway in Humans. J Neurosci 2018;38(43):9129–41.

Mirzadeh Z, Chapple K, Lambert M, Dhall R, Ponce FA. Validation of CT-MRI fusion for intraoperative assessment of stereotactic accuracy in DBS surgery. Mov Disord 2014;29:1788–95. https://doi.org/10.1002/MDS.26056.

Mitra P, Bokil H. Observed Brain Dynamics. New York: Oxford University Press; .

Mountcastle VB. The columnar organization of the neocortex. Brain 1997;120:701–22. https://doi.org/10.1093/BRAIN/120.4.701.

Narayanan RT, Egger R, Johnson AS, Mansvelder HD, Sakmann B, de Kock CPJ, Oberlaender M. Beyond Columnar Organization: Cell Type- and Target Layer-Specific Principles of Horizontal Axon Projection Patterns in Rat Vibrissal Cortex. Cereb Cortex 2015;25(11):4450–68.

Nauhaus I, Busse L, Carandini M, Ringach DL. Stimulus contrast modulates functional connectivity in visual cortex. Nat Neurosci 2009;12(1):70–6.

Obeso JA, Rodriguez-Oroz MC, Rodriguez M, Lanciego JL, Artieda J, Gonzalo N, Olanow CW. Pathophysiology of the basal ganglia in Parkinson's disease. Trends Neurosci 2000;23:S8–S19.

Okun M, Naim A, Lampl I. The Subthreshold Relation between Cortical Local Field Potential and Neuronal Firing Unveiled by Intracellular Recordings in Awake Rats. J Neurosci 2010;30:4440–8. https://doi.org/10.1523/JNEUROSCI.5062-09.2010.

Okun MS. Deep-Brain Stimulation for Parkinson's Disease. N Engl J Med 2012;367:1529–38. https://doi.org/10.1056/NEJMCT1208070.

Peters A, Sethares C. Myelinated axons and the pyramidal cell modules in monkey primary visual cortex. J Comp Neurol 1996;365:232–55. https://doi.org/10.1002/(sici)1096-9861(19960205)365:2<232::aid-cne3>3.0.co;2-6.

Quian Quiroga R, Nadasdy Z, Ben-Shaul Y. Unsupervised spike detection and sorting with wavelets and superparamagnetic clustering. Neural Comput 2004;16:1661–87. https://doi.org/10.1162/089976604774201631.

Quiroga-Varela A, Walters JR, Brazhnik E, Marin C, Obeso JA. What basal ganglia changes underlie the parkinsonian state? The significance of neuronal oscillatory activity. Neurobiol Dis 2013;58:242. https://doi.org/10.1016/J.NBD.2013.05.010.

Ray S, Maunsell JHR. Network Rhythms Influence the Relationship between Spike-Triggered Local Field Potential and Functional Connectivity. J Neurosci 2011;31(35):12674–82.

Rogers N, Hermiz J, Ganji M, Kaestner E, Kılıç K, Hossain L, Thunemann M, Cleary DR, Carter BS, Barba D, Devor A, Halgren E, Dayeh SA, Gilja V, Gershman SJ. Correlation Structure in Micro-ECoG Recordings is Described by Spatially Coherent Components. PLoS Comput Biol 2019;15(2):e1006769.

Shimamoto SA, Ryapolova-Webb ES, Ostrem JL, Galifianakis NB, Miller KJ, Starr PA. Subthalamic Nucleus Neurons Are Synchronized to Primary Motor Cortex Local Field Potentials in Parkinson's Disease. J Neurosci 2013;33(17):7220–33.

Shokoueinejad M, Park D-W, Jung Y, Brodnick S, Novello J, Dingle A, Swanson K, Baek D-H, Suminski A, Lake W, Ma Z, Williams J. Progress in the Field of Micro-Electrocorticography. Micromachines 2019;10(1):62.

Swan CB, Schulte DJ, Brocker DT, Grill WM. Beta Frequency Oscillations in the Subthalamic Nucleus Are Not Sufficient for the Development of Symptoms of Parkinsonian Bradykinesia/Akinesia in Rats. eNeuro 2019;6. https://doi.org/10.1523/ENEURO.0089-19.2019.

Swann NC, de Hemptinne C, Thompson MC, Miocinovic S, Miller AM, Gilron Ro'ee, Ostrem JL, Chizeck HJ, Starr PA. Adaptive deep brain stimulation for Parkinson's disease using motor cortex sensing. J Neural Eng 2018;15(4):046006. https://doi.org/10.1088/1741-2552/AABC9B.

Tinkhauser G, Pogosyan A, Little S, Beudel M, Herz DM, Tan H, et al. The modulatory effect of adaptive deep brain stimulation on beta bursts in Parkinson's disease. Brain 2017;140:1053–67. https://doi.org/10.1093/BRAIN/AWX010.

Wang DD, de Hemptinne C, Miocinovic S, Ostrem JL, Galifianakis NB, San Luciano M, Starr PA. Pallidal Deep-Brain Stimulation Disrupts Pallidal Beta Oscillations and Coherence with Primary Motor Cortex in Parkinson's Disease. J Neurosci 2018;38(19):4556–68.

Weaver FM, Follett K, Stern M, Hur K, Harris C, Marks WJ, et al. Bilateral Deep Brain Stimulation vs Best Medical Therapy for Patients With Advanced Parkinson Disease: A Randomized Controlled Trial. JAMA 2009;301:63–73. https://doi.org/10.1001/JAMA.2008.929.

Whitmer D, de Solages C, Hill B, Yu H, Henderson JM, Bronte-Stewart H. High frequency deep brain stimulation attenuates subthalamic and cortical rhythms in Parkinson's disease. Front Hum Neurosci 2012:155. https://doi.org/10.3389/FNHUM.2012.00155/BIBTEX.

Xing D, Yeh C-I, Shapley RM. Spatial Spread of the Local Field Potential and its Laminar Variation in Visual Cortex. J Neurosci 2009;29(37):11540–9.

Yang AI, Vanegas N, Lungu C, Zaghloul KA. Beta-Coupled High-Frequency Activity and Beta-Locked Neuronal Spiking in the Subthalamic Nucleus of Parkinson's Disease. J Neurosci 2014;34(38):12816–27.

Zhang S, Connolly AT, Madden LR, Vitek JL, Johnson MD. High-resolution local field potentials measured with deep brain stimulation arrays. J Neural Eng 2018;15(4):046019. https://doi.org/10.1088/1741-2552/AABDF5.